Table of Content

Supplemental Methods

NUMT exclusion from RNA-seq data: One source of contamination of our analyzed mtDNA gene expression data is sequencing reads of primitive mtDNA fragments that were transferred to the nDNA during the course of evolution (Hazkani-Covo et al. 2003; Mishmar et al. 2004). To control for such contamination, GTEx used nuclear mitochondrial pseudogene transcript sequences as their reference transcriptome (appears as mtXPN in the GTEx data, where X represents the mitochondrial gene and N stands for the number of the pseudogene). Therefore, reads that had higher similarity scores to any given pseudogene, as compared to the reference mtDNA gene, were excluded from the reads count for mtDNA-encoded genes. To further control for NUMTs, we used the normalized read counts (reads per kilo-base per million reads - RPKM) available in the GTEx consortium data files as our raw data. According to GTEx documentation, the read alignment distance was ≤6 (i.e., sequence alignments must not contain more than six mismatches), thus notably reducing possible contamination by NUMT reads.

RPKM to TPM conversion in RNA-seq data: The RPKM value for a given gene "i" in each library (each sample) was converted to TPM (Transcripts Per Million bases) as previously described (Hashimshony et al. 2012), using the following formula:

$$\mathrm{TPM_i} = \frac{\mathrm{RPKM_i}}{\text{Total library RPKM}} \mathrm{X}10^6$$

Control of RNA-seq data for age, gender and cause-of-death: The age variable was obtained as a continuous factor, whereas gender and cause-of-death were categorical factors. Dummy variables (1 for gender and 5 for cause-of-death) were used to correct for the effect of these factors on gene expression, while correcting for multiple testing. Finally, the residual TPM for each gene in each sample was calculated as the difference between the observed TPM and the TPM value predicted for this gene by the linear regression, considering phenotypic parameters (i.e. age, gender and cause-of-death).

Clustered heat maps construction: The median Spearman's rank correlation coefficient between the pairs of genes/transcripts under consideration were used to create a distance matrix for hierarchical clustering. Such clustering was obtained according to the similarity of the correlation of gene/transcript expression with other genes/transcripts under consideration. The correlation values were color-coded: red – positive correlation, blue – negative correlation. Non-significant or zero correlations are marked in white.

To construct heat maps for each of the analyzed tissues, we used the gene/transcript order that was obtained from the hierarchal clustering generated while analyzing the total expression pattern across all tissues. Additionally, while constructing tissue-specific correlation distance matrixes, we considered all samples available for the tested tissue.

Brain cell-type determination in single cell RNA-seq analysis: Cells were considered excitatory-neurons if they displayed higher maximal expression of the pan-glutamatergic marker-genes (*Slc17a6* and *Slc17a7*) than both the maximal expression of pan-GABAergic marker-genes (*Gad1*, *Gad2* and *Slc32a1*) and the non-neuronal marker genes (*Olig1*, *Gja1*, *Xdh*, *Ctss* and *Myl9*). Cells were considered inhibitory-neurons if they displayed higher maximal expression of the pan-GABAergic marker-genes as compared to both the maximal expression for pan-glutamatergic and non-neuronal marker-genes. Other cells were considered non-neuronal (Sugino et al. 2006; Tasic et al. 2016).

Statement - usage of human genome sequence versions (GRCh37 and GRCh38): The GTEx dataset is based on mapping of RNA-seq reads against the GRCh37/hg19; we used mapped reads which are publicly available, and do not have access to the restricted area of the GTEx data. As our analyses focus on gene expression correlation among OXPHOS genes, involving more than 80 genes that showed consistent and significant correlation values across and within tissues, it is safe to state that possible small changes in some of the genes' sequences, among different versions of the human genome, would not significantly alter our conclusions.

Structural predictions: Swiss-model server (https://swissmodel.expasy.org/) (default parameters) was used to predict the 3D structures of the discussed OXPHOS subunit alternatively spliced variants. In addition, we used Jpred 4 (http://www.compbio.dundee.ac.uk/jpred/), to predict secondary structures (default parameters) and assess their conservation between the canonical isoforms and the alternative ones.

References - supplemental methods

Hashimshony T, Wagner F, Sher N, Yanai I. 2012. CEL-Seq: single-cell RNA-Seq by multiplexed linear amplification. *Cell reports* **2**(3): 666-673.

Hazkani-Covo E, Sorek R, Graur D. 2003. Evolutionary dynamics of large numts in the human genome: rarity of independent insertions and abundance of post-insertion duplications. *Journal of molecular evolution* **56**(2): 169-174.

Mishmar D, Ruiz-Pesini E, Brandon M, Wallace DC. 2004. Mitochondrial DNA-like sequences in the nucleus (NUMTs): insights into our African origins and the mechanism of foreign DNA integration. *Hum Mutat* **23**(2): 125-133.

Sugino K, Hempel CM, Miller MN, Hattox AM, Shapiro P, Wu C, Huang ZJ, Nelson SB. 2006. Molecular taxonomy of major neuronal classes in the adult mouse forebrain. *Nature neuroscience* **9**(1): 99-107.

Tasic B, Menon V, Nguyen TN, Kim TK, Jarsky T, Yao Z, Levi B, Gray LT, Sorensen SA, Dolbeare T. 2016. Adult mouse cortical cell taxonomy revealed by single cell transcriptomics. *Nature neuroscience* **19**(2): 335-346.

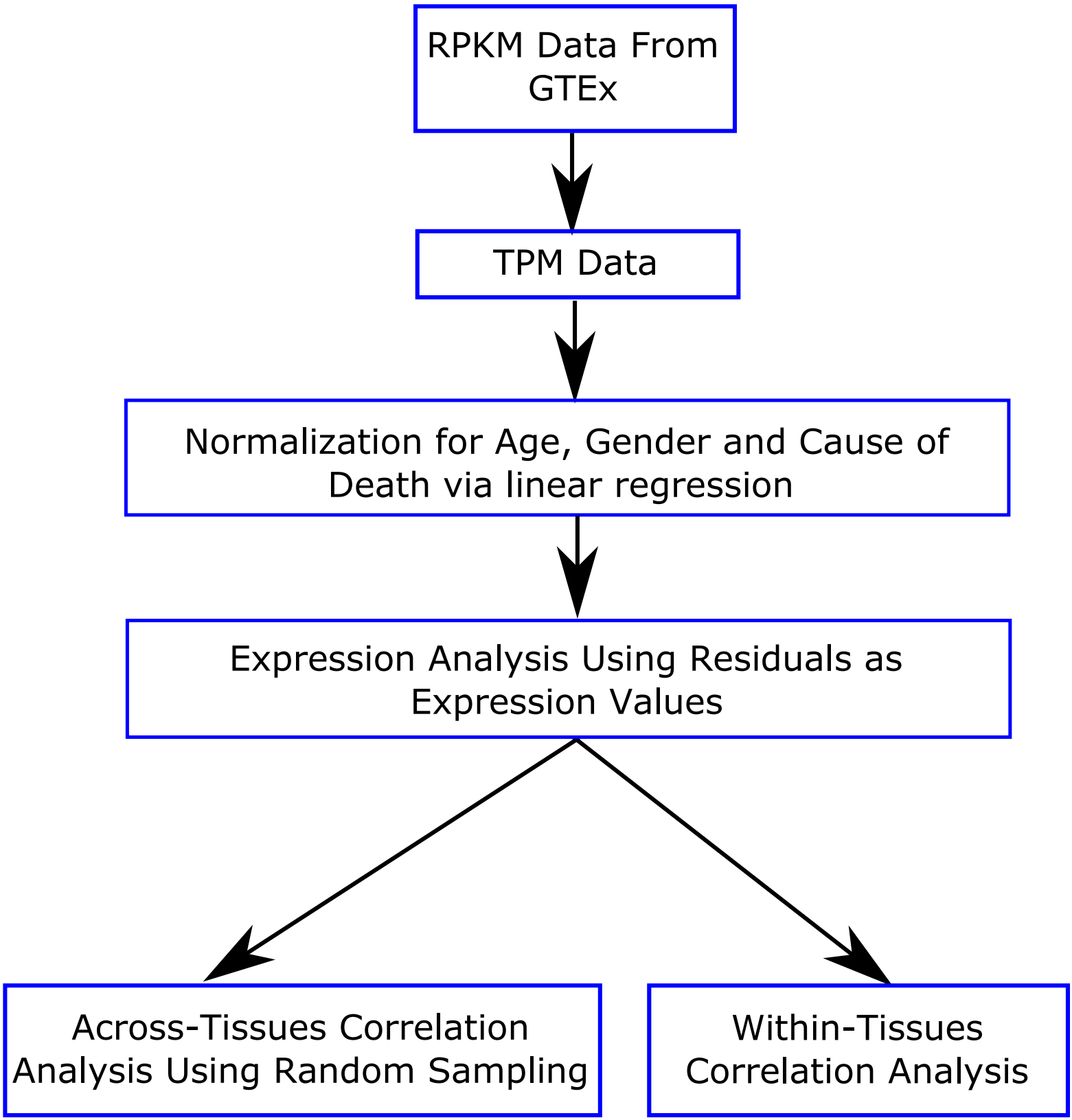

Figure S1. Workflow of the expression pattern correlation analysis. See also Supplemental Dataset S4 for Python scripts used during the analysis.

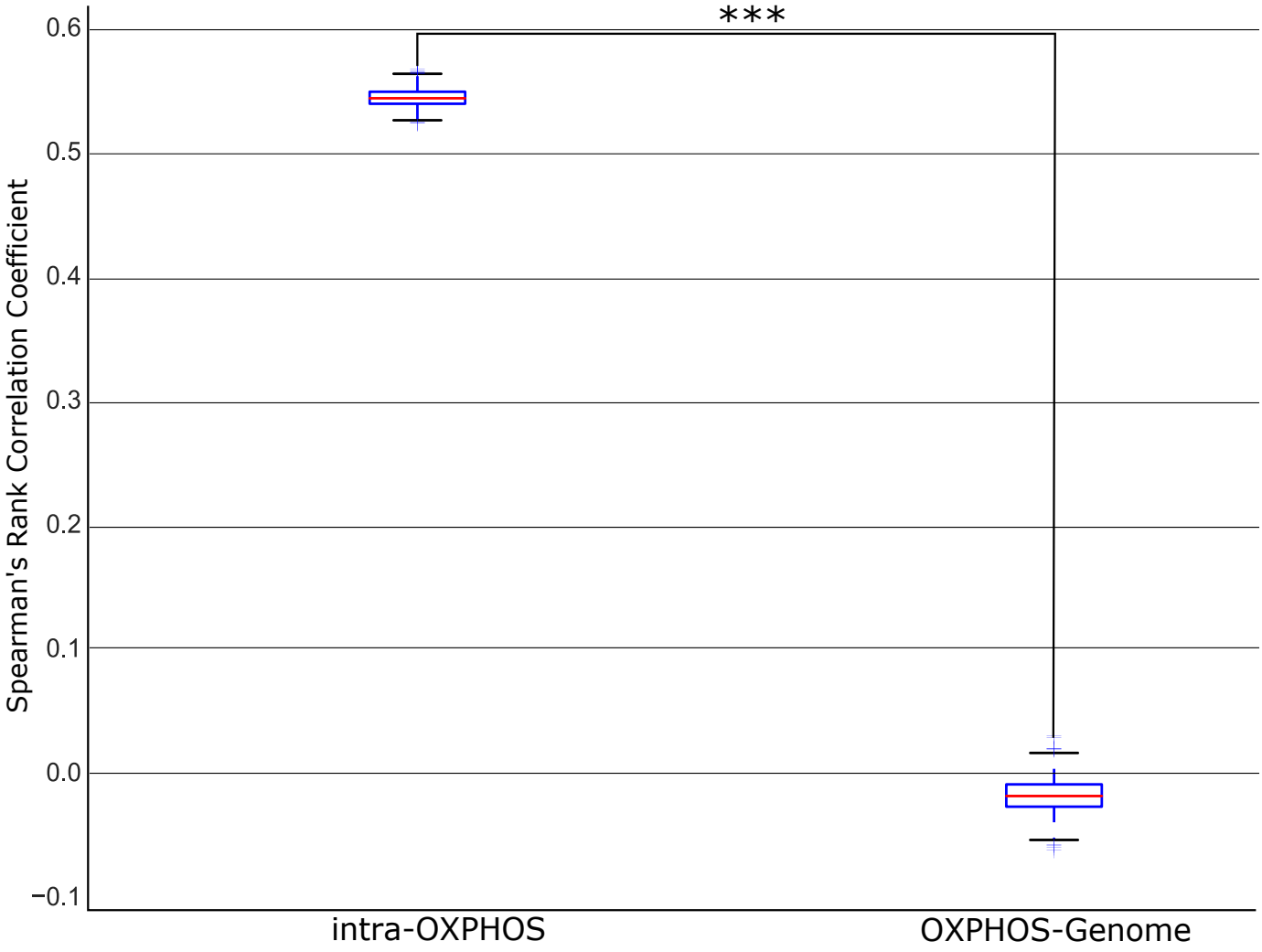

Figure S2. nDNA-encoded OXPHOS genes show significantly higher co-expression with mtDNA-encoded OXPHOS genes. A box-plot showing the values of the correlation coefficients between pairs of OXPHOS genes (intra-OXPHOS) and between OXPHOS genes and randomly chosen protein-coding genes (OXPHOS-Genome). *** $p < 1 \times 10^{-100}$.

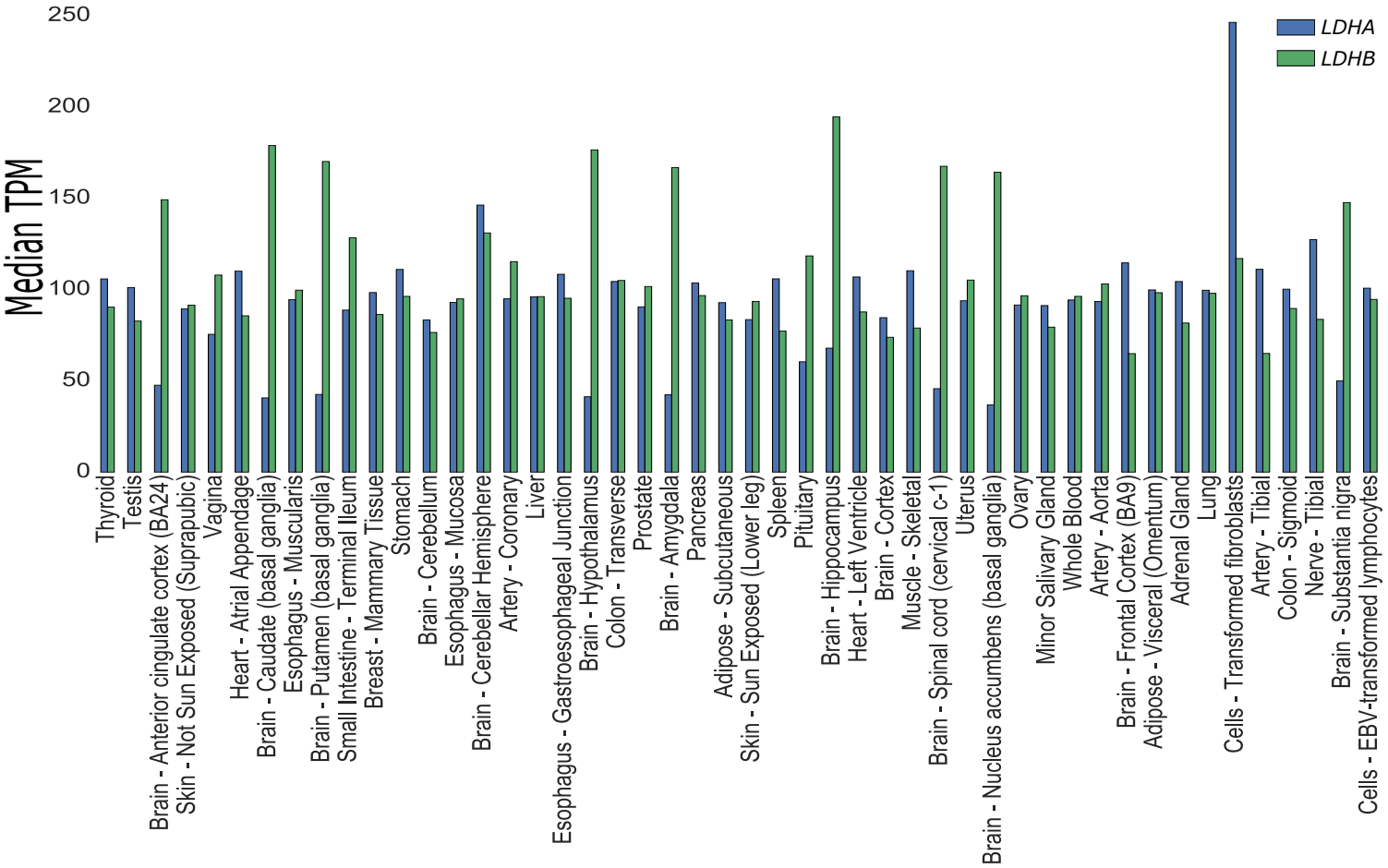

Figure S3. Expression of LDH subunits across human tissues. A bar-plot showing the median TPM values of the two LDH subunit-coding genes (*LDHA* and *LDHB*) across all human tissues inspected in this study.

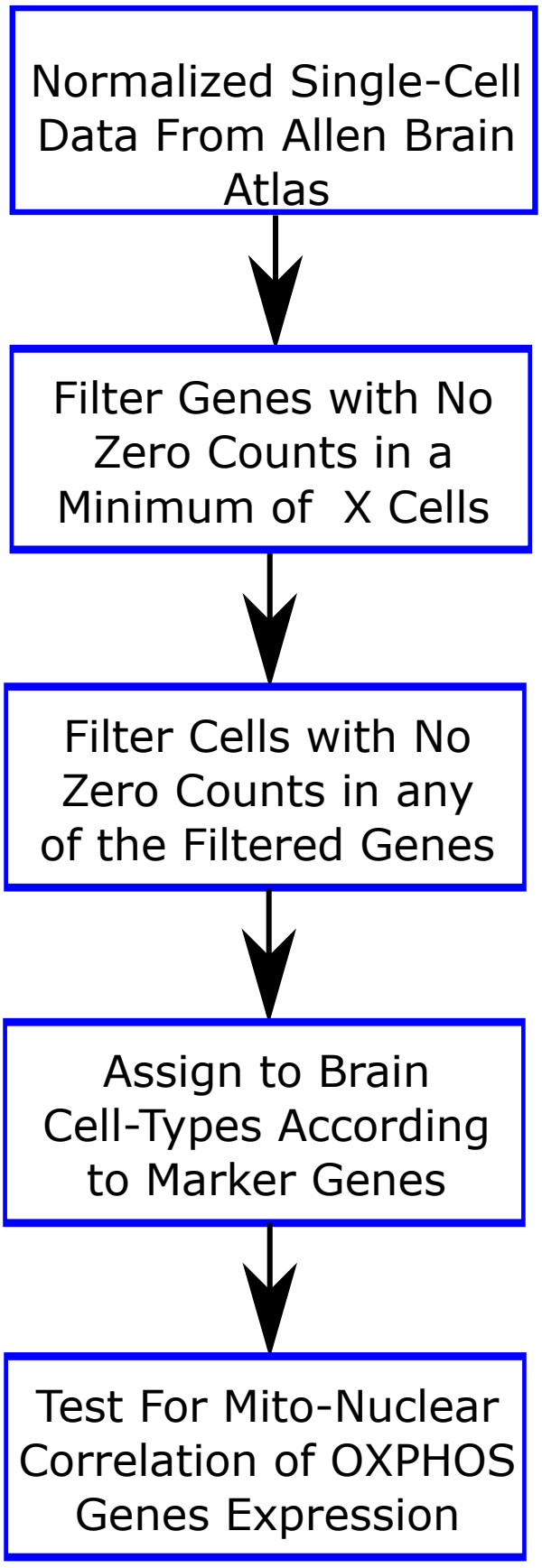

Figure S4. Workflow for single-cell RNA-seq data analysis for OXPHOS mito-nuclear correlation. See also ' Single-cell RNA-seq data analysis' under 'Methods'.

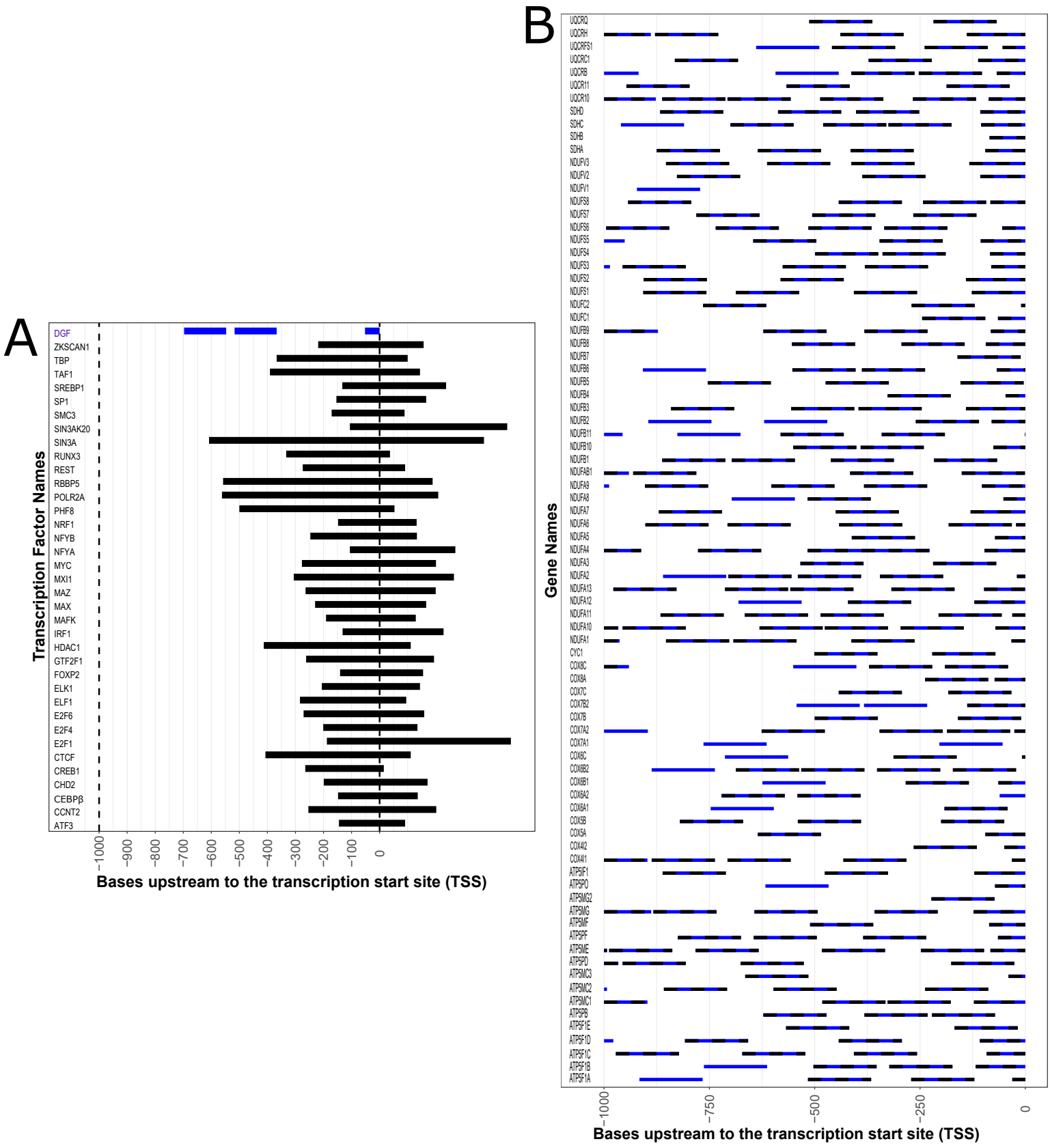
A
Transcription Factor Names
DGF
ZKSCAN1
TBP
TAF1
SREBP1
SP1
SMC3
SIN3AK20
SIN3A
RUNX3
REST
RBBP5
POLR2A
PHF8
NRF1
NFYB
NFYA
MYC
MXI1
MAZ
MAX
MAFK
IRF1
HDAC1
GTF2F1
FOXP2
ELK1
ELF1
E2F6
E2F4
E2F1
CTCF
CREB1
CHD2
CEBPβ
CCNT2
ATF3
−1000
−900
−800
−700
−600
−500
−400
−300
−200
−100
0
Bases upstream to the transcription start site (TSS)
B
Gene Names
UQCRQ
UQCRH
UQCRFS1
UQCRC1
UQCRB
UQCR11
UQCR10
SDHD
SDHC
SDHB
SDHA
NDUFV3
NDUFV2
NDUFV1
NDUFS8
NDUFS7
NDUFS6
NDUFS5
NDUFS4
NDUFS3
NDUFS2
NDUFS1
NDUFC2
NDUFC1
NDUFB9
NDUFB8
NDUFB7
NDUFB6
NDUFB5
NDUFB4
NDUFB3
NDUFB2
NDUFB11
NDUFB10
NDUFB1
NDUFAB1
NDUFA9
NDUFA8
NDUFA7
NDUFA6
NDUFA5
NDUFA4
NDUFA3
NDUFA2
NDUFA13
NDUFA12
NDUFA11
NDUFA10
NDUFA1
CYC1
COX8C
COX8A
COX7C
COX7B2
COX7B
COX7A2
COX7A1
COX6C
COX6B2
COX6B1
COX6A2
COX6A1
COX5B
COX5A
COX4I2
COX4I1
ATP5IF1
ATP5PO
ATP5MC2
ATP5MG
ATP5MF
ATP5PF
ATP5ME
ATP5PD
ATP5MC3
ATP5MC2
ATP5MC1
ATP5PB
ATP5F1E
ATP5F1D
ATP5F1C
ATP5F1B
ATP5F1A
−1000
−750
−500
−250
0
Bases upstream to the transcription start site (TSS)

Figure S5. Graphical representation of the in vivo identification of candidate promoters in nuclear DNA encoded OXPHOS genes.

(A) A map of the upstream region of a representative OXPHOS gene (NDUFA8) tested for TF binding in DNaseI Genomic Footprinting (DGF) sites. X-axis represent the positions in the promoter region, relative to the transcription start site (TSS). DGF sites are indicated by blue lines in the upper row and below, all the listed TFs binding to the 1000bp promoter region are shown, with their ChIP-seq peaks shown as black lines. Note that only TFs with a ChIP-seq peak overlapping a minimum of one DGF are indicated.

(B) Representation of the results for all nDNA-encoded OXPHOS genes. X-axis represent the positions in the promoter region, relative to the translation start site (TSS). DGFs are shown by blue lines if they do not overlap with any identified TF-binding peak in the ChIP-seq experiments and in black and blue lines if they overlap with at least one such TF-binding peak.

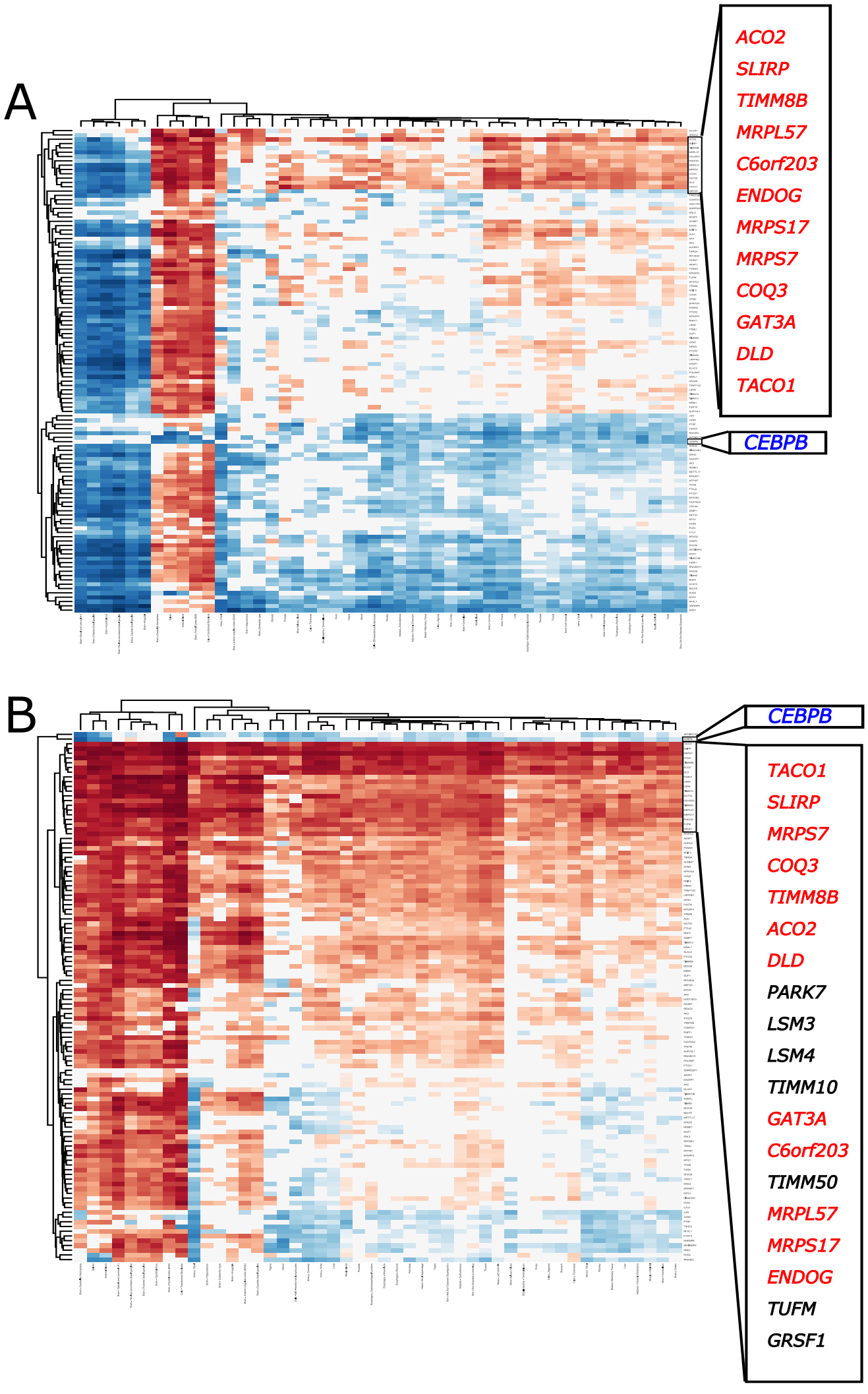
A
ACO2
SLIRP
TIMM8B
MRPL57
C6orf203
ENDOG
MRPS17
MRPS7
COQ3
GAT3A
DLD
TACO1
CEBPB
B
CEBPB
TACO1
SLIRP
MRPS7
COQ3
TIMM8B
ACO2
DLD
PARK7
LSM3
LSM4
TIMM10
GAT3A
C6orf203
TIMM50
MRPL57
MRPS17
ENDOG
TUFM
GRSF1

Figure S6. The candidate mito-nuclear OXPHOS expression regulators correlation with OXPHOS genes. Heat maps representing the median correlation values of the different candidate regulators, with the mtDNA-encoded (A) and nDNA-encoded (B) OXPHOS genes.

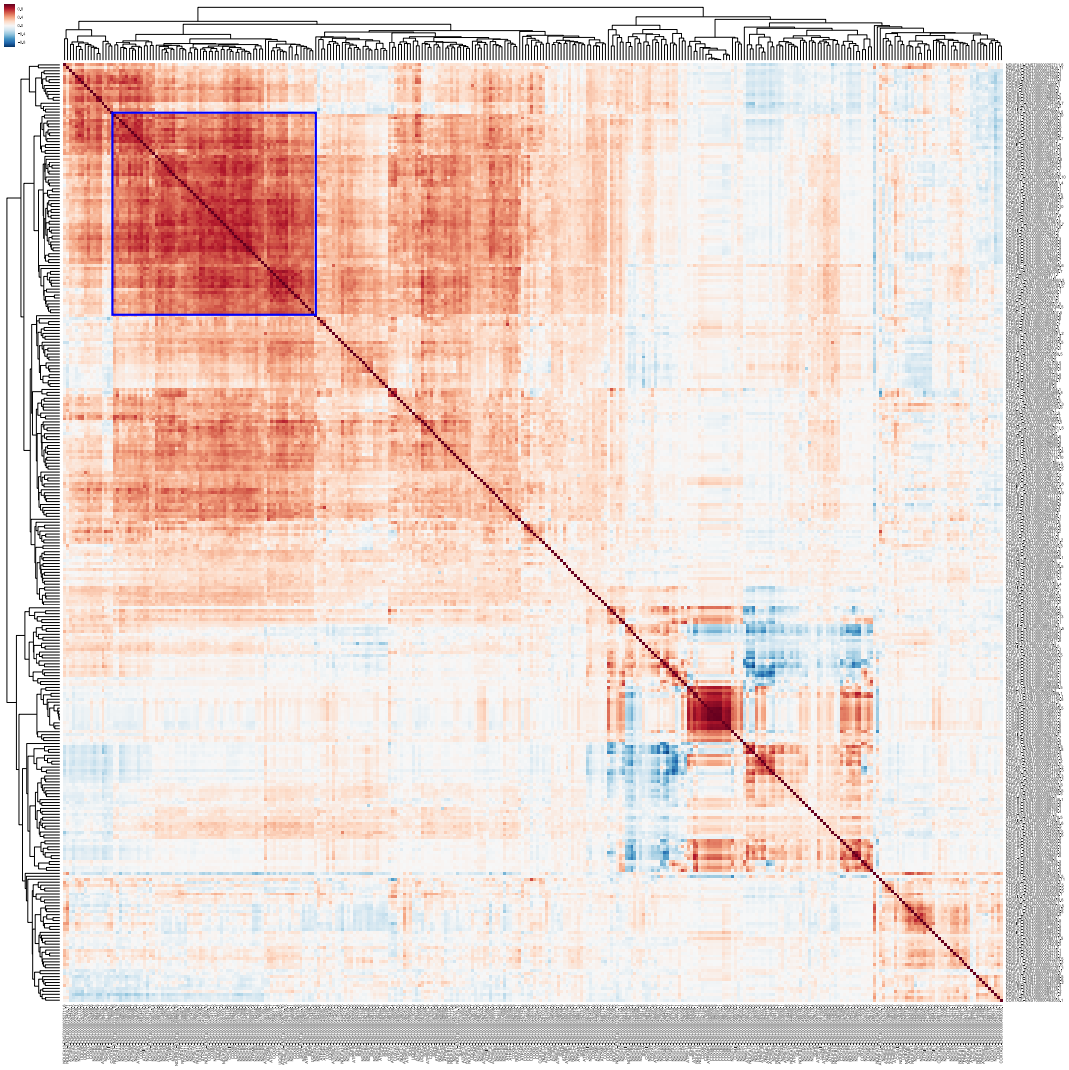

Figure S7. OXPHOS genes splice-variants correlations and the 'main OXPHOS transcript cluster'. A heat map of correlation values for the expression of all OXPHOS transcripts. The 'main OXPHOS transcript cluster' is marked with a blue square. A key for the color code of the Spearman's correlation coefficients is shown in top left corner.

A

NDUFA2

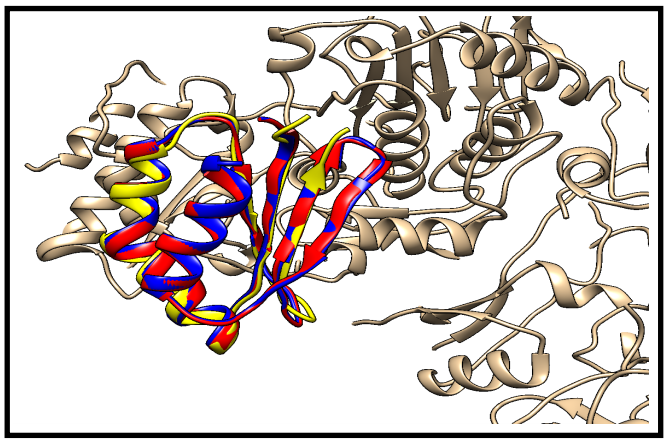

NDUFB11

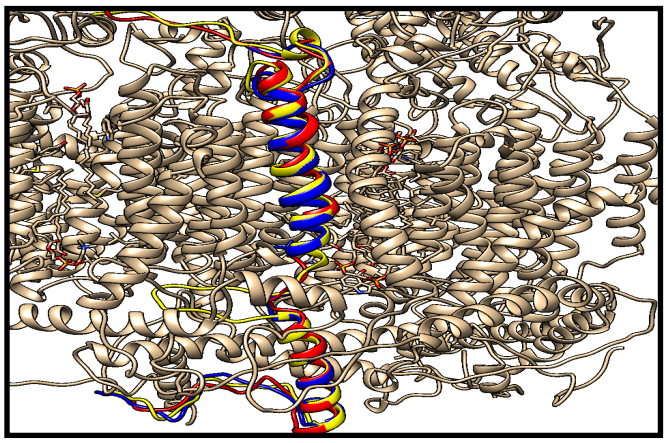

NDUFB6

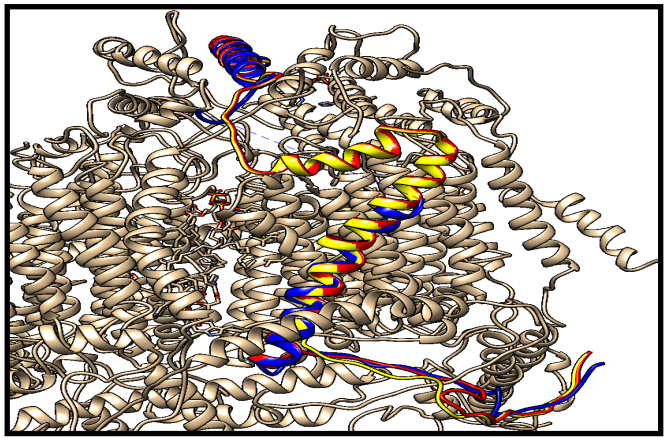

B

NDUFA3

Canonical:

```
VGAFLKNAWDKEPVLVVSFVVGGLAVILPPLSPYFKYSVMINKATPYNYPVPVRDDGNMPDVPSHPQDPQGPSLEWLKKL
-HHHHHHH-----EEEEHHHHHHHHEEE-------HHHHHH-----------------------------------HHHHH--
```

Alternative:

```
KCRSRRLPQECLGQGASAGRVLRRRGPRCNSAPIEPLLQVLRHDQQGHALQLPSARP
--------HHHH-----HHHHHHH---------HHHHHHHHHH------EE------
```

ATP5MF

Canonical:

```
MASVGECPAPVPVKDKKLLEVKLGELPSWILMRDFSPSGIFGAFQRGYYRYYNKYINVKKGSISGITMVLACYVLFSYSFSYKHLKHERLRKYH
----------EE-----------HHHHHHHHHHHHHHHH-EEEE-------HHHHHHHHHHHHHHHH-------------
```

Alternative:

```
MASV------VPVKDKKLLEVKLGELPSWILMRDFSPSGIFGAFQRGYYRYYNKYINVKKGSISGITMVLACYVLFSYSFSYKHLKHERLRKYH
----xxxxxx-----------------------HHHHHHHHHHHHHHH--EEEE-------
```

Figure S8. Structural comparison between the suggested splice-isoforms and the canonical spliceisoforms. (A) 3D models comparing the structures of the canonical (red), alternative (yellow) and sheep (blue) isoforms of NDUFA2, NDUFB6 and NDUFB11. (B) Secondary structures prediction for the alternative splice-isoforms of NDUFA3 and ATP5MF, that lacked a homolog with high sequence similarity and a solved 3D structural model, to the canonical isoforms of these subunits.

Supplemental Datasets legends and links

Supplemental Dataset S1: Correlation heat maps for OXPHOS genes and splice variants expression patterns in 48 human tissues. https://figshare.com/s/cc5cb8e5107cba4da7e3

Supplemental Dataset S2: Correlation matrices for expression patterns of OXPHOS genes and splice variants of OXPHOS genes in 48 human tissues. https://figshare.com/s/818279d849951436ee72

Supplemental Dataset S3: Relative correlation heatmaps for splice-variants of genes with more than one transcript highly OXPHOS correlated across tissues. https://figshare.com/s/223934fe6e99ab3bf528

Supplemental Dataset S4: Python scripts for raw data conversion, normalization and co-expression analysis. https://figshare.com/s/83db1452d76b266e0e34